"Cloud slicing" retrievals of the methane concentration in the planetary boundary layer from CHARM-F XCH$_4$ measurements over the Northern Scandinavian wetlands

Mathieu Quatrevalet, Andreas Fix, Martin Wirth, Tanja Bodenbach, Philipp Rossi

Institut für Physik der Atmosphäre, Deutsches Zentrum für Luft- und Raumfahrt (DLR)
D-82234 Oberpfaffenhofen, Germany
Lead Author e-mail address: Mathieu.Quatrevalet@dlr.de

Abstract: Airborne or spaceborne Integral Path Differential Absorption (IPDA) lidar has the potential to deliver the highly accurate column measurements of trace gases that are needed to reduce the uncertainties on the surface fluxes of anthropogenic greenhouse gases. Among its advantages over passive remote sensing is the very narrow field of view, which makes it possible to exploit "cloud holes" at all spatial scales to increase the coverage. Moreover, in a broken cloud field scenario, it is possible to turn the IPDA lidar into a pseudo-range-resolved lidar and retrieve the average trace gas concentration in the atmospheric layer below the clouds by combining partial columns down to the cloud tops and total columns down to the ground. This is usually referred to as "cloud slicing". Here we report on an attempt to apply cloud slicing on methane data from DLR's airborne IPDA lidar, CHARM-F. The data was acquired on the 23rd of August 2021 over the northern Scandinavian wetlands in the frame of the MAGIC 2021 campaign. We show that cloud slicing enables to overcome some issues with the instrument's performance during the campaign and that the retrieved methane concentration in the boundary layer matches well with vertical in-situ profiles acquired during the same flight.

1.   Introduction

The IPDA lidar for simultaneous measurements of carbon dioxide and methane of the German Aerospace Centre (DLR), CHARM-F, was originally designed to fly on D-ADLR, DLR's High-Altitude, Long-Range research aircraft (HALO), in order to fulfill its role as a technology demonstrator for future spaceborne missions and validation tool for the upcoming MERLIN mission. Since being presented for the first time at the ILRC in 2010 [1], it has accumulated over 200 flight hours on this platform. In the frame of the 2021 activities related to the MAGIC (Monitoring of Atmospheric composition and Greenhouse gases through multi-Instrument Campaigns) initiative of the French CNES and CNRS [5], an opportunity arose to fly it for the first time on another platform, F-HMTO, the ATR-42 of the Service des Avions Français Instrumentés pour la Recherche (SAFIRE), which operated from Kiruna, Sweden in August 2021 for a campaign focusing on methane emissions from arctic wetlands and lakes.

Due to a number of factors that are outlined in paragraph 2, the performance of CHARM-F on F-HMTO during MAGIC 2021 was not as satisfactory as during the previous and subsequent flight campaigns on D-ADLR. Nevertheless, one flight over a 80x60 km wetland area south of Gällivare in the afternoon of August, 23ʳᵈ provides an interesting case study for so-called "cloud slicing" retrievals thanks to the partial coverage by small-scale convective clouds, a scenario where the ability of the lidar to use both cloud tops and the ground as a scattering surface makes it possible to retrieve the methane concentration within the Planetary Boundary Layer (PBL).

2.   Instruments and data

CHARM-F, its data processing chain and its general performance have been described in detail in previous ILRC contributions and elsewhere [1, 2, 3, 5]. A critical feature of the instrument is that it sports two receivers per trace gas, producing two largely independent datasets that can be cross-checked for instrumental biases. One receiver is equipped with a 20-cm aperture and a four-quadrant PIN

photodiode and the other with a 6-cm aperture and an APD photodiode, and will be referred to in the following as the "PIN" receiver and the "APD" receiver, respectively. Figure 1 shows the XCH4 time series derived from each receiver with a 3-s gliding average for the stabilized portion of the flight at 7.6 km altitude over the wetlands. Time-varying biases between the APD and PIN channel can be seen, as well as slow drifts followed by jumps, with magnitudes up to 40 ppb.
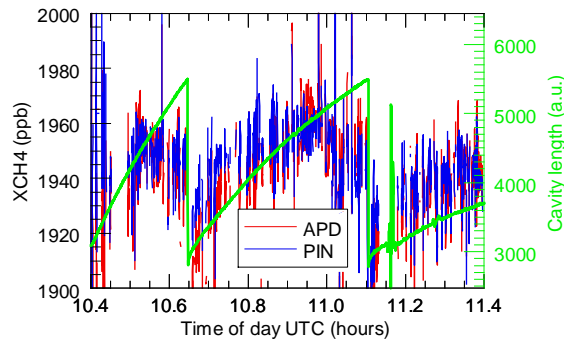

Figure 1. Time series of the XCH4 values derived from the APD (red) and PIN (blue) receiver signals of CHARM-F; time series of the methane transmitters' OPO cavity length.

The reason for these time-varying biases is linked to the fact that, compared to range-resolved DIAL lidars, IPDA lidars have to substitute one of the two atmospheric range bins that are normally used in the DIAL equation with internal calibration signals. It was already posited in [3] that asymmetries between the effective online and offline transmission of the optical path (which cancel out in the range-resolved case) are incorrectly accounted for by the CHARM-F calibration path. The latter has been carefully designed [4] to minimize this risk, however ground-based measurements after MAGIC 2021 have pointed to asymmetric trimming of the laser footprint by the field of view as the main culprit. This is confirmed in the MAGIC data and on Figure 1 through the correlation of the measurement with the actively controlled cavity length of the Optical Parametric Oscillator (OPO) at the heart of the transmitter, due to non-parallel movement of the associated piezo-element.

Shorter flight durations on F-HMTO compared with HALO, a generally lower flight altitude, and frequent altitude changes and thus temperature/pressure changes in the cabin (preventing thermal stabilization of the transmitter) enhanced the problem, together with the fact that the laser divergence was set to about half to two thirds of the field of view.

The histogram of the scattering surface elevation on the left-hand side of Figure 2, reflects the fact that the afternoon weather on the day of the flight was dominated by convective clouds between 1.5 km and 2 km, with some higher clouds near 3.3 km. On the right-hand side of Figure 2, the distribution of the three corresponding SSE clusters are mapped along the flight path for the stabilized portion of the flight. A balanced mix of low clouds and cloud-free scenes can be observed in all legs except the northernmost.
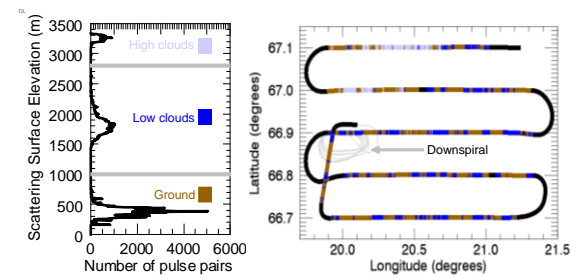

Figure 2. Left: histogram of the SSE from CHARM-F data. Right: distribution of the three SSE classes along the stabilized flight path, and flight path corresponding to the down-spiral.

Also shown on Figure 2 is the flight path for the down-spiral that was flown in order to acquire vertical profiles of atmospheric parameters, in particular trace gas measurements from SAFIRE's Picarro G2410. The methane measurement is plotted on Figure 3 as a function of altitude, along with the calculated CHARM-F weighting function.
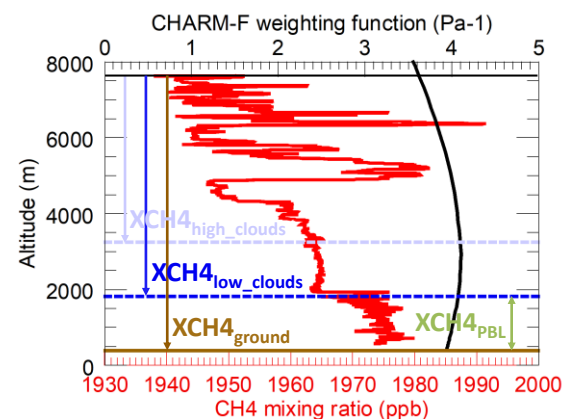

Figure 3. Red: Methane volume mixing ratio as a function of altitude during the down-spiral. Black: calculated CHARM-F pressure weighting function as a function of altitude. See text for other details.

Also shown on Figure 3 with horizontal dashed lines are the altitude of the stabilized flight legs (black), mean altitude of the high cloud layer (dashed light blue) and low cloud layer (dashed blue), as well as the mean ground altitude during the spiral (solid brown). The profile confirms that the low clouds match the top of the PBL, with a clear jump of more than 10 ppb due to the wetland emissions. Using the knowledge of the CHARM-F weighting function, it is possible to calculate the expected column-averaged methane mixing ratios in the total column $XCH4_{ground}$, in each partial column $XCH4_{high\_clouds}$ and $XCH4_{low\_clouds}$, and in the PBL, $XCH4_{PBL}$. The corresponding values are listed in Table 1.

Table 1. Calculated "in-situ XCH4"

Column	Value (ppb)
$XCH4_{high\_clouds}$	1957.4
$XCH4_{low\_clouds}$	1959.1
$XCH4_{ground}$	1960.7
$XCH4_{PBL}$	1974.3

3. Method and results

Figure 4 illustrates three possible scenarios/approaches with an IPDA lidar in the presence of convective clouds marking the top of the PBL.
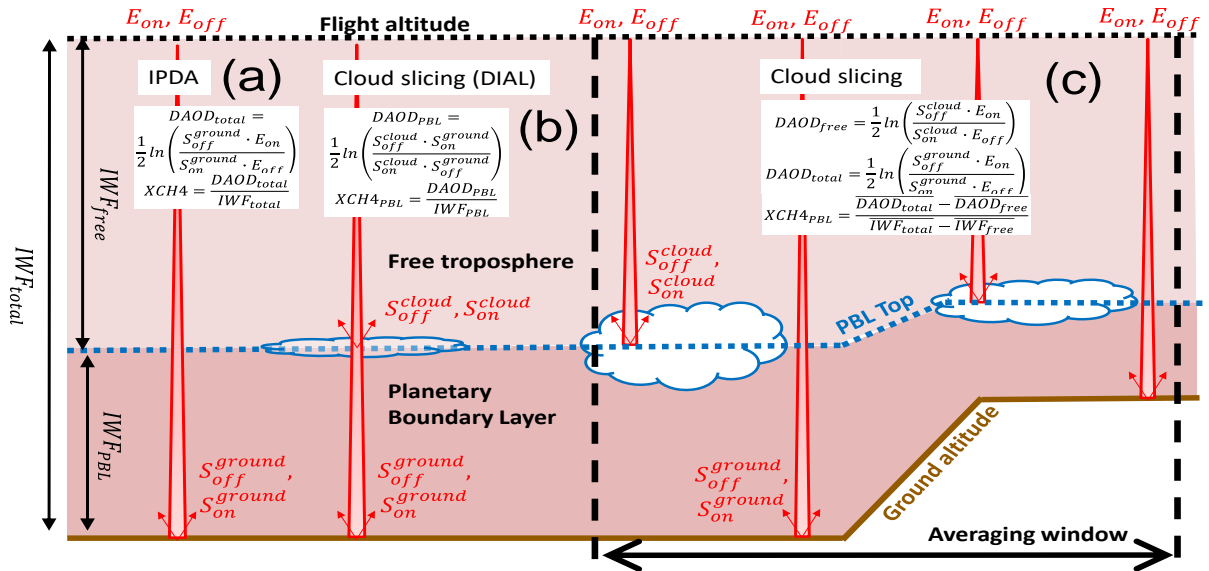
(DAOD) is calculated from the two ground echoes and the two calibration signals, and can be converted to XCH4 by dividing by the Integrating Weighting Function (IWF). Case (b) illustrates the presence of an optically thin cloud, whereby thin means that a first pair of backscatter signals is produced by the cloud, while a sufficient portion of the laser energy reaches the ground to produce a second pair of backscatter signals. This allows to apply the DIAL equation directly to the cloud top and ground echoes, without a need for internal calibration signals, with at least some of the asymmetries mentioned in paragraph 2 being canceled out. And finally, case (c) illustrates a broken field of optically thick clouds, providing a mix of partial and total column measurements. Both (b) and (c) enable "cloud slicing", i.e. potentially give access to $XCH4_{PBL}$. However, while a significant portion of pulse waveforms in the CHARM-F data do contain both a ground and a cloud echo, the current version of the CHARM-F processing chain only allows for the strongest echo to be processed.

We therefore turn to approach (c), which requires the definition of an averaging window over which ground and cloud top measurements are combined via the "cloud slicing equation". For this we first listed the approximately 700

Figure 4. Illustration of the cloud slicing concept in the context of an IPDA lidar with a convective cloud layer.

Case (a) illustrates the class ical, cloud-free, total column IPDA retrieval where the Differential Atmospheric Optical Thickness

ground-low cloud transitions (cf Figure 2) in the data, then applied the cloud slicing equation within a window of increasing width centered around these transitions. For each averaging window width, we computed the median and standard deviation over all the 700 resulting $XCH4_{PBL}$ values. The result is shown on Figure

5 for both the APD and the PIN channels, along with the median and standard deviation of the 700 values obtained by applying the "classical" IPDA equation to the partial (cloud) and total (ground) columns and averaging within the same windows.

It can be first observed that the standard deviation is a factor of 5 to 10 worse for $XCH4_{PBL}$ than for the partial and total columns, due to the fact that the DAOD in the PBL is a factor 4 smaller than in the total column, and that it requires twice as many individual measurements to be computed.
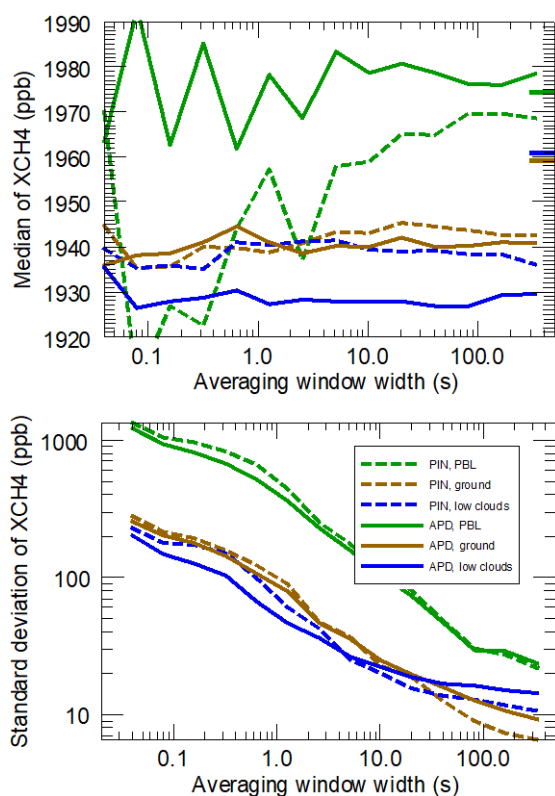

Figure 5. Top: median of the XCH4 values calculated using the method described in paragraph 3 for the APD (solid) and the PIN (dashed) channel. Bottom: standard deviations of the XCH4 values as a function of the averaging window width.

On the top panel of Figure 5, the calculated "in-situ" values from Table 1 have been positioned on the right-hand vertical axis in order to compare them with the lidar measurements, assuming that the down-spiral is representative of the whole 80 km x 60 km area. While both $XCH4_{ground}$ and $XCH4_{low\_clouds}$ converge to values that are 20 to 30 ppb, or 1 to 1.5% away from the expected value, $XCH4_{PBL}$ converges for both channels and for averaging widths

longer than about 1 minute to within 5 ppb or 0.25% of the expected value, a factor five improvement of the accuracy. Thus, not only does the cloud slicing approach give access to the elevated methane concentration in the PBL: it can restore the self-calibrating effect that is a natural property of range-resolved DIAL lidars, even when using ground and cloud top echoes from different pulse pairs.

4.   References

[1] Quatrevalet, M., Amediek, A., Fix, A., Kiemle, C., Wirth, M., Büdenbender, C., Schweyer, S., Ehret, G., Hoffmann, D., Meissner, A. Löhring, J. and Luttmann, J. (2010) *CHARM-F: The Airborne Integral Path Differential Absorption Lidar for Simultaneous Measurements of Atmospheric CO2 and CH4.* 25th International Laser Radar Conference (ILRC), 05.-09. Juli 2010, St. Petersburg, Russia.

[2] Amediek, A., Ehret, G., Fix, A., Wirth, M., Büdenbender, C., Quatrevalet, M., Kiemle, C., and Gerbig, C. (2017) *CHARM-F - a new airborne integrated-path differential-absorption lidar for carbon dioxide and methane observations: measurement performance and quantification of strong point source emissions.* Applied Optics, **56** (18), 5182-5197. DOI: 10.1364/AO.56.005182.

[3] Amediek, A., Ehret, G., Fix, A., Büdenbender, C., Quatrevalet, M., Kiemle, C. (2017) *Performance of CHARM-F - the Airborne Demonstrator for MERLIN.* 28th International Laser Radar Conference, 25.-30 June 2017, Bucarest, Romania. doi: 10.1051/epjconf/201817601002.

[4] Fix, A., Quatrevalet, M., Amediek, A., Wirth, M. (2018) *Energy Calibration of Integrated Path Differential Absorption Lidars.* Applied Optics, 57 (26), pp. 7501-7514. Optical Society of America. doi: 10.1364/AO.57.007501.

[5] Fix, A., Amediek, A., Büdenbender, H. C., Ehret, G. Kiemle, C., Quatrevalet, M., Wirth, M., Wolff, S., Bovensmann, H., Butz, A., Galkowski, M. and Gerbig, C., Jöckel, P., Marshall, J., Necki, J., Pfeilsticker, K., Roiger, A.-E., Swolkien, J. and Zöger, M. (2020*) CH4 and CO2 IPDA Lidar measurements during the COMET 2018 airborne field campaign.* 29th International Laser Radar Conference (ILRC), 237, 03005/1-4. doi: 10.1051/epjconf/202023703005.

[6] Crevoisier, C., Bès, C-, Joly, L., Té, Y, Ramonet, M.. Herbin, H., Catoire, V., Fix, A., Cézard, N., Bourdon, M. (2021) *Overview of the MAGIC initiative for GHG and future plans.* IWGGMS 17 (17th International Workshop on Greenhouse Gas Measurements from Space), 14.-17. Jun. 2021. https://cce.nasa.gov/iwggms17